Ultrafast laser control of electron dynamics in atoms, molecules and solids

Matthias Wollenhaupt and Thomas Baumert*

Received 5th September 2011, Accepted 19th September 2011
DOI: 10.1039/c1fd00109d

Exploiting coherence properties of laser light together with quantum mechanical matter interferences in order to steer a chemical reaction into a pre-defined target channel is the basis of coherent control. The increasing availability of laser sources operating on the time scale of molecular dynamics, *i.e.* the femtosecond regime, and the increasing capabilities of shaping light in terms of amplitude, phase and polarization also on the time scale of molecular dynamics brought the temporal aspect of this field to the fore. Since the last *Faraday Discussion* (*Faraday Discussion 113*, *Stereochemistry and control in molecular reaction dynamics*) devoted to this topic more than a decade ago a tremendous cross-fertilization to neighbouring "quantum technology disciplines" in terms of experimental techniques and theoretical developments has occurred. Examples are NMR, quantum information, ultracold molecules, nonlinear spectroscopy and microscopy and extreme nonlinear optics including attosecond-science. As pointed out by the organizers, this meeting brings us back to chemistry and aims to assess recent progress in our general understanding of coherence and control in chemistry and to define new avenues for the future. To that end we will in the Introductory lecture first shortly review some aspects of coherent control. This will not be fully comprehensive and is mainly meant to give some background to current experimental efforts of our research group in controlling (coherent) electronic excitations with tailored light fields. Examples and perspectives for the latter will be given.

1 Introduction

Coherent control is a fascinating facet of femtochemistry.[1,2] Traditionally femtochemistry deals with laser-based real-time observations of molecular dynamics by making use of light pulses that are short in comparison to the molecular time scale. Coherent control goes beyond this *ansatz*. Here one seeks to actively exert microscopic control over molecular dynamics at the quantum level on intrinsic time scales. The goal is to steer any type of light-induced molecular processes from an initial state to a pre-defined target state with high selectivity and with high efficiency. Progress in this fast expanding research field is documented in recent textbooks,[3–5] review articles[6–22] and special issues.[23–27]

Suitable tools to achieve this goal are shaped femtosecond optical laser pulses in amplitude, phase and polarization (see Fig. 1 (a)), where different shaping techniques are reviewed in the literature.[11,28–31] Precision pulse shaping down to the zeptosecond regime has been reported recently, opening the perspective of controlling electron dynamics with unprecedented precision (see Fig. 1 (b)).[32]

Universität Kassel, Institut für Physik und CINSaT, Heinrich-Plett-Str. 40, 34132 Kassel, Germany. E-mail: baumert@physik.uni-kassel.de; Fax: +49 561 804 4453; Tel: +49 561 804 4452

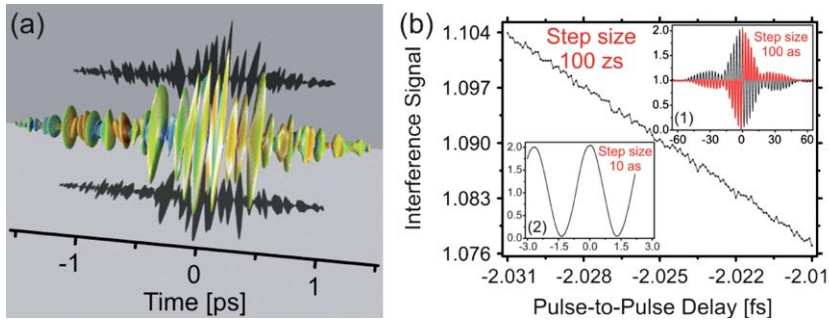

Fig. 1 (a) Example of an optimal laser pulse—shaped in amplitude, phase and polarization—employed to maximize the K_2^+ ion yield from Resonance Enhanced Multi Photon Ionization (REMPI) of potassium dimers K_2 exploiting the vectorial properties of light–matter interaction in a feedback learning loop (adapted from ref. 48). In the three-dimensional representation the electric field amplitudes are indicated by the sizes of the corresponding ellipses and the instantaneous frequencies are indicated by colors. The black shadows represent the amplitude envelopes of the two orthogonal polarization components. (b) Example of zeptosecond precision pulse shaping. Measured interference signal of two time delayed pulses created by a high precision pulse shaper. Inset (1) shows the interferogram with a step size of 100 as, whereas inset (2) shows a zoom into the interferogram with a step size of 10 as. The main figure shows a measurement within the time delay interval from -2.031 fs to -2.0199 fs measured with a step size of 100 zs. The obtained time resolution ($2\,\sigma$) is 300 zeptoseconds (1 zs = 1 zeptosecond = 10^{-3} attosecond = 10^{-6} femtosecond, figure adapted from ref. 32).

Optimized light fields can be found for example by employing adaptive feedback learning loops[33–39] or by fine tuning the parameters of physically motivated pulse shapes,[40–44] where experimentally determined quantum control landscapes[45,46] can help identifying underlying physical mechanisms especially in the strong-field regime. Shifting the focus to spectroscopy, the understanding of different dynamical mechanisms can lead to sets of physically motivated pulse shapes, where the parameters of these pulse shapes can be adapted to the molecules under study either systematically or evolutionary. This spectroscopy *ansatz* would go beyond the typical pulse sequence spectroscopy with Fourier limited pulses and it was suggested to name this approach quantum control spectroscopy.[18,47]

In contrast to weak-field (perturbative) quantum control schemes where the population of the initial state is approximately constant during the interaction with the external light field, the strong-field (non perturbative) regime is characterized by efficient population transfer. Adiabatic strong-field techniques such as rapid adiabatic passage (RAP) or stimulated Raman adiabatic passage[49,50] are employed for instance with laser pulses in the picosecond[11,51–53] to nanosecond domain allowing for population transfer with unit efficiency in quantum state systems. Only recently were these techniques transferred to the femtosecond regime. For example, selectivity based on (dynamic Stark shifted) RAP combined with high efficiency was demonstrated in an atomic ladder system with the help of chirped laser pulses,[54] and piecewise adiabatic passage was demonstrated in an atomic two level system with chirped pulse sequences.[55] Furthermore, it was shown that the effects of the dynamic Stark shift reducing the excitation efficiency can be compensated with temporally structured pulses.[56] Switching the electronic population to different final states with high efficiency *via* selective population of dressed states (SPODS) is a further fundamental resonant strong-field effect as the only requirement is the use of intense ultrashort pulses exhibiting time varying phases such as phase jumps[57–60] or chirps.[43,61]

The modification of the electronic potentials due to the interaction with the electric field of the laser pulse has another important aspect pertaining to molecules, as the nuclear motion can be significantly altered in light induced potentials. An experimental review devoted to the topic of small molecules in intense laser fields focusing

mainly on H_2 excitation and fragmentation dynamics is given in ref. 62. Experimental examples for modifying the course of reactions of neutral molecules after an initial excitation *via* altering the potential surfaces can be found in ref. 63 and 64 where the amount of initial excitation on the molecular potential can be set *via* Rabi type oscillations.[65] Nonresont interaction with an excited vibrational wavepacket can in addition change the population of the vibrational states.[66]

Although a high degree of excitation can be achieved *via* Rabi oscillations, this approach is not attractive for efficient coherent control schemes as the resonant Rabi oscillation period is proportional to the scalar product of the electric dipole moment times the electric field of the laser pulse. As a consequence, different excitation levels are achieved due to the intensity distribution within the focal area of a typical Gaussian laser beam and due to different orientations of the molecules in a typical isotropic sample. This is why the above mentioned adiabatic strong-field approaches are especially important as they are robust against these effects.

Conceptually most of the mechanisms underlying coherent control have been demonstrated in the gas phase, where the latest highlight is quantum control of bond formation in a catalytic surface reaction.[67] However, as relevant chemistry, biology and medicine is typically taking place in the liquid phase, laser control of dissolved molecules is most promising for applications. The field is reviewed in ref. 16 where direct control of ground state vibrational excitation,[68] control of energy flow in large light harvesting molecules,[69] control of isomerization processes[70,71] and optical discrimination of molecules with nearly identical absorption profiles[72–74] are prominent examples. Examples of robust and efficient electronic excitation of molecules especially in the liquid phase are rare (see ref. 75 and 76 for theoretical discussions related to earlier experiments[36,77]).

In this Introductory lecture we focus on (coherent) electronic excitation with shaped laser pulses. We first discuss our experiments devoted to create designer electron wave packets in the continuum by making use of the electronic structure of atoms together with polarization shaped laser pulses. We present our tomography method to reconstruct the three-dimensional electron distributions and hint at possible applications. We then focus on coherent strong-field excitation. This is the regime beyond perturbative descriptions of light matter interactions and below the regime where the ionization probability reaches unity. It is the regime where Rabi cycling is important and we highlight the importance of controlling resonant processes in this regime. Two examples are given. We start discussing experiments in the gas phase, where a first laser pulse creates a charge oscillation with maximum coherence. In the region of valence electron excitations, these charge oscillations are on the order of one femtosecond and making use of these coherences for reaction control requires a second pulse which interacts with this coherence with attosecond precision. We then turn to experiments in the liquid phase where we discuss strong-field scenarios for adiabatic population transfer. These are derived from simulations based on our strong-field experiments making use of physically motivated pulse parameterizations for adiabatic strong-field interactions. Finally we briefly present our experiments demonstrating control of ionization processes in dielectrics for material processing on the nanometre scale. Typical excitation densities are in the range of 10^{21} electrons cm^{-3} and collision times on the order of one femtosecond prevent coherence introduced from the light field from being exploited. Nevertheless, we show that shaping temporal asymmetric profiles address multi photon ionization and electron-electron impact ionization in a different fashion.

2. Tomography of designer electron wave packets

In this chapter the main focus is to make use of the electronic structure of matter together with polarization shaped laser pulses in order to create designed electron wave packets in the continuum. The techniques developed, open new routes to

chemical analytics as well as to the measurement of photoelectron angular distributions in the molecular frame.

The basis of this approach was the demonstration of interferences of free electron wave packets generated by a pair of identical, time-delayed, femtosecond laser pulses which ionized excited atomic potassium.[78] In that experiment two different schemes were investigated: threshold electrons produced by one-photon ionization with parallel laser polarization and above threshold ionization electrons produced by a two-photon transition with crossed laser polarization. As the measurement does not provide knowledge on the "which way information" *i.e.* whether the system is ionized by the first laser pulse or the second, double pulse photo ionization is a Young's double slit experiment in the time domain and naturally interferences have to occur. The time evolution of these interferences can be understood in a Wigner description[79] and the interferences can be used for pulse characterization[79] also in the attosecond regime.[80]

Making use of resonance enhanced multi photon ionization (REMPI) with amplitude, phase and polarization shaped laser pulses, the continuum can be structured by addressing different quantum mechanical states during the REMPI process as for example: the central wavelength and the spectral width of the laser will in a perturbative regime address different final states due to energy conservation and selection rules, where the number of possibilities is rapidly increasing with the number of photons; in addition non-perturbative fields induce Stark shifts that are reflected in the resonant case in the Autler Towns Splitting[81] and can be controlled with amplitude[32,57] and phase shaped[59,82] laser pulses; in the non-resonant case dynamic Stark shifting gives access to contributions from off-resonant states that can be selectively controlled for example with chirped laser pulses[54] as well.

Therefore, by tailoring the state of polarization, a high degree of control on the angular and energy distributions of ultrashort free-electron wave packets is obtained by interference of multiple excitation and ionization pathways.[83] The generated photoelectron angular distributions (PADs) were recorded with the velocity map imaging (VMI) technique.[84,85] These PADs are so called Abel projections of (in general) complex-shaped wave packets. If the detector plane contains an axis of symmetry—as for example linearly polarized light with the polarization vector parallel to the detector plane or circularly polarized light with the direction of the propagation of the light parallel to the detector plane—the three-dimensional distribution can be derived *via* different inversion methods from the two-dimensional projections.[86–89] For polarization shaped laser pulses these approaches do not work. However, measurements of PADs by rotating the complex polarization-shaped laser pulse delivers all information required for tomographic techniques to reconstruct the three-dimensional electron wave packets.[90] With the help of this technique designed complex-shaped three-dimensional electron wave packets are accessible to direct measurements. Two examples of such designer electron wave packets are given. In Fig. 2 an adaptively optimized designer electron wave packet is displayed together with its tomographic reconstruction. Fig. 3 shows a reconstruction from excitation with a "v" and polarization shaped pulse (see Fig. caption).[91]

In the recent past PADs have proven to be essential to analyze ionization dynamics and (neutral) molecular dynamics[85,92] because they contain highly differential information. The tomography approach presented could be used for example to determine radial phase shifts of partial waves in ionization processes or to give better understanding in strong-field ionization.[93] Combining the tomography approach with molecular alignment techniques[94,95] would give direct access to molecular frame PADs complementing coincidence techniques[96,97] that can give this information in the case of direct fragmentation processes. Another route to obtain molecular frame PADs could make use of alignment *via* excitation by exploiting the vectorial properties of light matter interaction. For such an approach polarization shaped laser pulses are again attractive as demonstrated for optimizing REMPI processes in the potassium dimer.[48] In that experiment—due to the

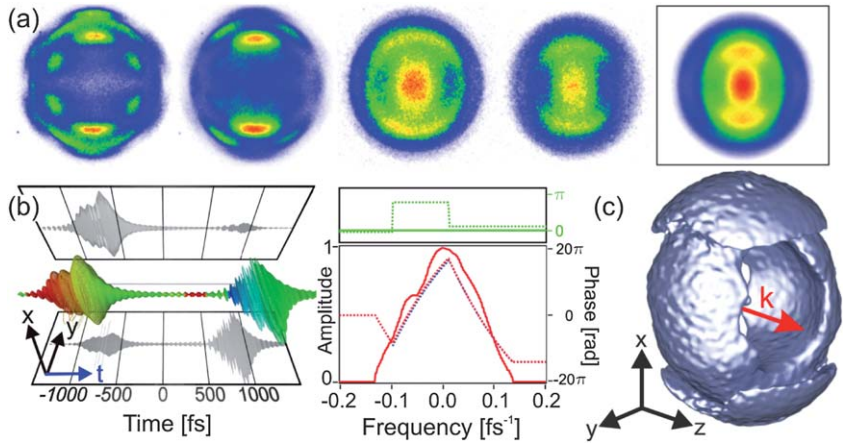

Fig. 2 Adaptive optimization of photoelectron angular distribution (PAD) measured by velocity map imaging (VMI) from resonance enhanced multi photon ionization (REMPI) of potassium atoms with polarization shaped femtosecond laser pulses employing an evolutionary algorithm. (a) The target PAD (boxed) is iteratively approximated by optimization of the spectral phase of the laser pulse. Results during the optimization process are shown from left to right for the individuals no. 1, 130, 260 and the optimized result at no. 597. (b, left): Optimized polarization shaped femtosecond laser pulse which yields the target PAD in a three-dimensional representation and (b, right) optimized pulse in the frequency domain. The pulse parameters are: central wavelength of 790 nm, FWHM pulse duration of 30 fs and peak intensity of about 3×10^{11} W cm^{-2}. For the optimization, the spectral phase modulation function was parameterized by piecewise linear functions in order to delay different spectral bands with respect to each other and, in addition, a relative phase between both polarization components was applied in order to control the ellipticity of individual spectral bands. (c) Three-dimensional tomographic reconstruction of the designed free electron wave packet which optimally reproduces the two-dimensional target PAD. Analysis of the pulse shape reveals that the optimized wave packet is created by two time-delayed slightly elliptically polarized sub pulses containing different spectral components (adapted from M. Krug PhD thesis[91]).

symmetry of the electronic states involved in the REMPI process—the light had to adapt its polarization state to parallel and perpendicular transitions during the excitation resulting in complex polarization shaped pulses (see Fig. 1 (a)).

Now lets turn to analytics. Given the argument that angular and energy distributions of ultrashort free-electron wave packets are obtained by interference of multiple excitation and ionization pathways being sensitive to the electronic structure, the combination of polarization shaping and velocity map imaging could be a sensitive analytic tool for molecular recognition in the gas phase where especially chiral recognition is attractive.[98] To that end we have started experiments on randomly oriented enantiomers of camphor and fenchone, and preliminary data were presented in the Introductory lecture. We ionized the corresponding enantiomers *via* a 2 + 1 REMPI process with circular polarized light and observed asymmetries in the forward-backward direction of ejected electrons. These experiments build on the pioneering synchrotron work on photoelectron circular dichroism by Laurent Nahon and Ivan Powis with coworkers[99] where a striking forward-backward electron ejection asymmetry was found in one-photon ionization of camphor enantiomers with circular polarized light. Note that sensitive chiral recognition is a prerequisite for chiral purification schemes based on coherent control techniques. For the latter see for example the work by Moshe Shapiro and coworkers and references therein.[100]

3. Control out of states of maximum electronic coherence

In this section the main focus is on a specific strong-field effect *i.e.* photon locking which is one realization of control *via* selective population of dressed states

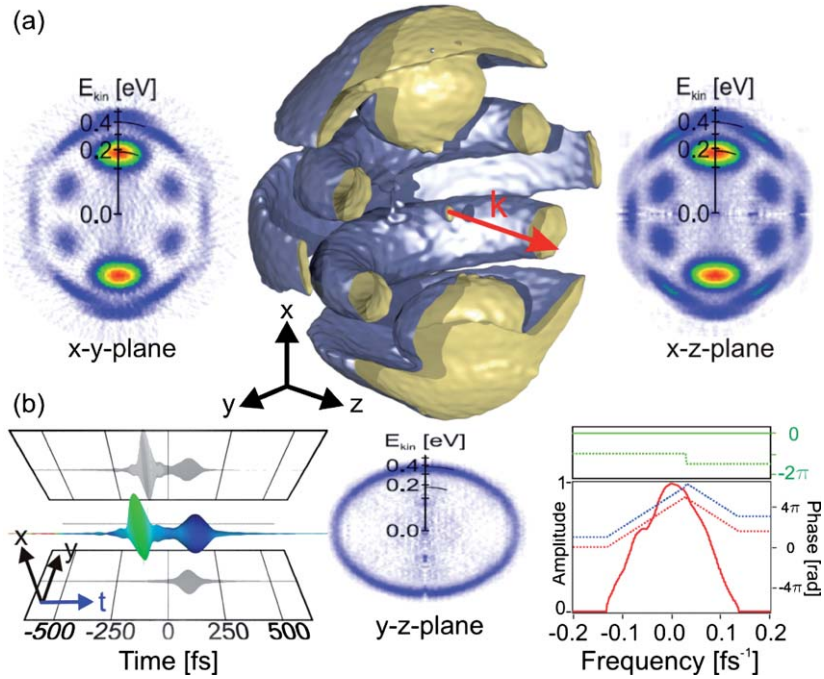

Fig. 3 Example of a designed electron wave packet in the continuum resulting from REMPI of potassium atoms employing combined "v"-shaped spectral phase modulation and polarization shaping.[83] (a) Three-dimensional tomographic reconstruction of a designed free electron wave packet obtained by multiple measurements of PADs with the complex polarization-shaped laser pulse rotated about the propagation vector using a $\lambda/2$ plate (see ref. 90 for further details on the tomography technique). The cuts through the origin in the x-y-plane, the x-z-plane and the y-z-plane illustrate the rich structure of the wave packet. The f-orbital type structure of the wave packet is attributed to the linearly polarized pulse in the x direction whereas the "hat" results from the circularly polarized delayed blue detuned pulse. (b) Pulse shape in time and frequency domain (the central wavelength is 790 nm, the FWHM pulse duration 30 fs and the peak intensity about 4×10^{12} W cm^{-2}). The "v"-shaped spectral phase advances the intense red spectral band and retards the weaker blue spectral band. Due to the additional phase jump, the first pulse is linearly polarized along the x-axis whereas the second pulse is circularly polarized (adapted from M. Krug PhD thesis[91]).

(SPODS). In analogy to vibrational wave packet control an oscillating charge distribution with maximum amplitude *i.e.* a state of maximum electronic coherence is created with a first laser pulse and by timing a second laser pulse with sub cycle precision (down to the zeptosecond regime, see Fig. 1 (a)) switching of population to different final states in atoms and molecules with high efficiency is demonstrated (see Fig. 4, Fig. 5 and Fig. 6). SPODS can also be used to measure decoherence phenomena as suggested in ref. 101 and beautifully exploited on single molecule spectroscopy.[102]

Motivation for these investigations stems from the enormous success of closed loop adaptive control experiments (see introduction) often resulting in complicated and not uniquely defined pulses. In many cases the first excitation band in such scenarios is reached after non-resonant absorption of a few photons, requiring already strong-fields. Taking into account that during a multi-photon process regions with an increasing density of electronic states are reached, suggests that strong-field coupling effects are present under such excitation conditions. Since the resonant control pathways will always dominate the controlled dynamics, resonant control scenarios will be important when looking for mechanisms. Increasing

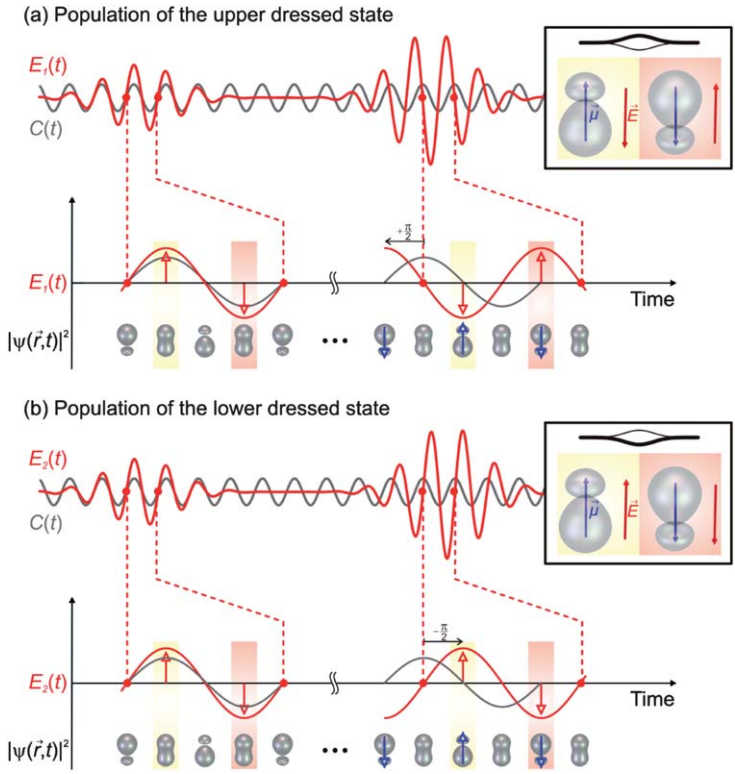

Fig. 4 Coherent control by photon locking employing a two pulse sequence displayed in a spatio-temporal picture illustrating population of the upper dressed state (a) and the lower dressed state (b). A comparison of a reference carrier oscillation $C(t)$ (grey sinusoidal curve with constant amplitude) in phase with the first weaker pulse of the driving pulse sequence $E(t)$ (red) highlights the phase shift of the second pulse in the sequence. The first pulse creates a state of maximum coherence exemplified by the electronic wave packet $|\psi(r, t)|^2$, *i.e.* a charge oscillation with maximum amplitude. The asymmetry in the charge distribution gives rise to an oscillating electric dipole moment μ (blue arrow), initially following the driving force with a phase shift of $\pi/2$. By timing the second pulse with sub cycle precision its phase relative to the induced atomic charge oscillation is controlled in order to realize photon locking. In scenario (a) the phase of the second pulse in the sequence $E_1(t)$ is shifted by $+\pi/2$. This carrier phase jump (introduced by suitable *spectral* phase modulation) shifts the electric field and the induced charge oscillation *out of phase*, *i.e.* during the second pulse both vectors E and μ oscillate anti parallel throughout. In this configuration the populations are *locked* and, hence, the dipole oscillation remains unaltered. This applies also to scenario (b), in which the carrier phase jump of $-\pi/2$ shifts the electric field *in phase* with the dipole moment such that subsequently both vectors oscillate parallel during the second pulse. The anti parallel (parallel) configuration maximizes (minimizes) the energy $W = -\mu\ E$ of the interacting system which is equivalent to selective population of the upper (lower) dressed state. SPODS *via* photon locking is an example of coherent control by tailoring of the phase of the laser field with respect to the ultrafast electron dynamics. A detailed discussion of SPODS in the spatio-temporal picture is presented in ref. 43.

significance for resonant control schemes is also given when ultra broad spectra for coherent control are employed. These come along with the ability to produce and shape shorter and shorter pulses.

In general, strong laser fields give rise to an energy splitting of the resonant state into two (so called dressed) states in the order of $\hbar\Omega$, where Ω describes the Rabi frequency. The decisive step in switching among different final electronic states is realized by the manipulation of dressed state energies and dressed state populations.

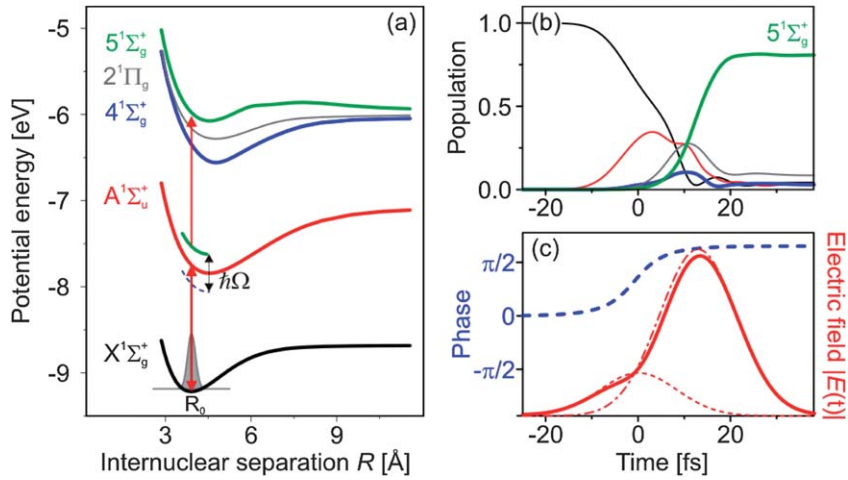

Fig. 5 Wave packet simulation on control of population in potassium dimers K_2 by SPODS. (a) Multi-photon excitation scheme for potassium dimers and (b) time evolution of the population in the X $^1\Sigma_g^+$-state (black), the A $^1\Sigma_u^+$-state (red), the 4 $^1\Sigma_g$-state (blue), the 2 $^1\Pi_g$-state (grey) and the 5 $^1\Sigma_g^+$-state (green). The first part of the pulse creates a superposition state of the X $^1\Sigma_g^+$ and the A $^1\Sigma_u^+$ states. During the second part of the pulse the X $^1\Sigma_g^+$ and the A $^1\Sigma_u^+$ states are locked in a state of maximum coherence. The optical phase controls which of the dressed states (indicated at R_0) energetically separated by $\hbar\Omega$ is selectively populated. Absorption of another photon leads to population transfer to one of the (non-resonant) states 4 $^1\Sigma_g^+$ and 5 $^1\Sigma_g^+$. Selective population of the upper dressed state with subsequent transition to the 5 $^1\Sigma_g^+$-state is illustrated. (c) Absolute value of the envelope of the electric field of the pulse sequence $|E(t)|$ (red) and its temporal phase function (blue dashed). The sequence consists of two pulses (red dashed) with a FWHM of 14.1 fs and a central wavelength of 830 nm separated by of 12.1 fs. The second stronger pulse has a peak intensity of approximately 7×10^{11} W cm^{-2} and exhibits a relative phase jump of approximately $\pi/2$. At this delay and phase the upper dressed state is selectively populated leading to resonant excitation of the 5 $^1\Sigma_g^+$-state with about 80% efficiency (adapted from ref. 104).

By suitable shaping of the driving laser field, it is possible to populate one of these two (dressed) states, *i.e.* to realize selective population of dressed states (SPODS). Effectively, the population of a single dressed state amounts to a controlled energy shift of the resonant state into a desired direction. By the variation of the laser intensity the energy splitting can be controlled, and thus a particular target state among the manifold of final states is addressed. Experimentally strong-field coherences in the potassium 4p–4s transition were excited with shaped laser pulses and the selective population of dressed states was monitored during the interaction by a perturbative two-photon ionization process into the continuum with the help of photoelectron spectroscopy. Dressed state population is reflected in the amplitude of the corresponding Autler–Towns component, where energy shifts of the order of several hundred meV have been observed[57] highlighting again the importance for strong-field control of chemical reactions. In a multitude of experiments on the potassium atom it was found that continuous temporal phase variations[43,61] as well as temporal phase discontinuities[43,45,57,58,82,101] lead to SPODS and only so called "real" pulses (pulses with a constant temporal phase except for π-jumps which merely represent a change of the sign of the envelope) do not exhibit this effect[61] because the pulse area theorem applies. In such cases, which are challenging to realize experimentally, weak-field control schemes can be extended to the strong-field regime.[103]

Robustness of SPODS, *i.e.* insensitivity to reasonable changes in the pulse energy, was found for chirped pulses[43,61] as well as for pulses with step phase modulation[59]

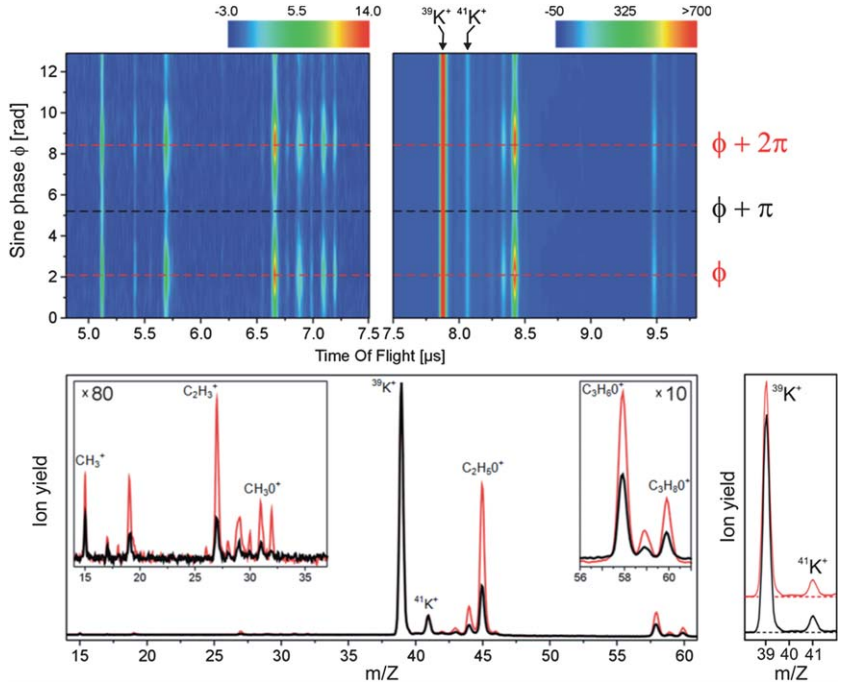

Fig. 6 Control of the fragmentation of isopropyl alcohol (C_3H_8O) using a pulse sequence. Upper panel: False color representation of TOF—mass spectra from the dissociation of isopropyl alcohol. Pulse sequences are created by a sinusoidal spectral phase modulation function $\varphi(\omega) = 0.5 \sin[50 \text{ fs } (\omega\text{-}2.4 \text{ fs-}1) + \phi]$ of a 10 μJ, 30 fs, 785 nm femtosecond laser pulse. The phase ϕ is varied within 4π. Lower panels: sections through the mass spectra at $\phi \approx 2$ rad (red) and $\phi \approx 5.5$ rad (black) exhibit a pronounced variation of the molecular ion yield. At the mass of $m =$ 45 u ($C_2H_5O^+$) a variation in the molecular ion yield by a factor of 3 is observed. The insets show a magnification of the spectra. The atomic ion yield of $^{39}K^+$ and $^{41}K^+$ measured simultaneously as a reference shows no variation with the phase (right). The observed phase dependence hints to ultrafast switching of coherent electronic excitation in a molecule by SPODS (adapted from ref. 109).

and an extension of SPODS to a three-state system was studied recently.[60] The conclusion is that coherent electronic excitation of resonant states with shaped laser pulses leads in general to SPODS in this atomic model system. Many different pulse shapes lead to comparable dressed state energy shifts and dressed state population. If operative in larger systems as well this could explain why in closed loop experiments optimzed pulses often do not exhibit a unique structure.

In order to investigate this aspect, photon locking—being one specific realization of SPODS—was studied also with respect to molecules. This strong-field quantum control scheme—based on concepts originally developed in NMR (spin-locking)[105]—makes explicit use of temporal phase changes within the pulse and was demonstrated experimentally using nanosecond laser pulses.[106,107] We extend these techniques to the femtosecond time scale with relevant applications to coherent control. The main physical picture behind photon locking is as follows: a first resonant interaction creates an oscillating charge distribution with maximum amplitude and by timing a second interaction with sub cycle precision switching of population to different final states is achieved (see Fig. 4 and Fig. 5). As the charge oscillations are in the order of one femtosecond for typical valence excitations control has to be performed with attosecond precision. Sub 10 as precision in such an electron control scheme has recently been demonstrated.[32] Direct control of valence bond electron

dynamics with attosecond pulses seems to be difficult, as the corresponding photon energy is usually not compatible with valence electron excitation. However, direct monitoring of valence electron dynamics with attosecond techniques has been achieved.[108]

Regarding molecules, wave packet simulations on a generic diatomic molecule[58] and on the potassium dimer[104] have been performed, implementing a photon locking pulse sequence. The simulations confirmed the selectivity and tunability of SPODS in the presence of nuclear motion and ultrafast efficient population transfer to target states (see Fig. 5). Preliminary experimental data on the potassium dimer were presented in the Introductory lecture. Indications for control out of coherently excited electronic states with subcycle precision were presented and data on intensity variations confirmed that the expected strong-field scenario is operative. No indications of weak-field control *via* higher order spectral interferences were observed in accordance with the findings on atoms.[57] Further indications that SPODS in general and photon locking as a specific example are important strong-field mechanisms come from theoretical considerations: in paper 11 of this meeting (DOI: 10.1039/c1fd00031d) Philipp von den Hoff, Markus Kowalewski and Regina de Vivie-Riedle concluded after investigating selective excitation in the potassium dimer with the help of optical control theory (OCT): "the SPODS mechanism is an optimal solution in the OCT search space. From the properties of the OCT algorithm it is known that high quality control and robust solutions are found even for complex quantum systems including a large number of control variables. In this sense the SPODS can be regarded as a robust way to control the selective population of higher lying electronic states, opening a wide spectrum of applications ranging form reaction control within molecules up to discrimination between different molecules in a mixture." When studying the excitation of ground-surface vibrational motion while minimizing radiation damage Ronnie Kosloff, Audrey Dell Hemmerich and David Tannor found that photon locking is a key ingredient in that control scenario.[110]

For applications to chemistry, a validation of such a coherent control strategy on larger molecules is helpful. As a first step, we investigated the mass spectra—measured with a time of flight spectrometer—from dissociation of isopropyl alcohol using a photon locking sequence.[109] The results shown in Fig. 6 show pronounced variations in the molecular ion yield upon variations of the temporal phase in the pulse sequence. In these experiments the simultaneously measured ion yield from potassium atoms showed no significant variations. This result confirms that no spectral/spatial cross-sensitivities are introduced by our pulse shaper. The observations show that control of the molecular dynamics of isopropyl alcohol is exerted by the optical phase of the shaped pulse. The phase dependence of the signal is hinting to a SPODS mechanism, however, systematic studies on the intensity dependence for a final proof have not been performed so far.

4. Adiabatic population transfer on molecules in solution

In this section we show that physically motivated pulse parameterizations based on frequency sweeps together with temporal pulse envelope asymmetries help to identify possible mechanisms for adiabatic population transfer in molecules. Joint wave packet motion (JOMO) and eigenstate preparation are presented as strong-field processes complementing frequency ordering followed by pump dump scenarios[111] and picosecond ultrabroadband positive chirp approaches.[75]

Rapid adiabatic passage is a well known concept in atomic physics where the complete population from one state is transferred to another state.[50] In the simplest case a detuned laser of sufficient pulse area sweeps through a resonance in order to achieve complete population transfer. Experimental realisations down to the picosecond[51] and femtosecond[54,61] regime have been reported and extensions to artificial atoms, *i.e.* quantum dots were demonstrated as well.[112]

As already mentioned in the introduction, a high degree of excitation can also be achieved *via* Rabi oscillations, however, this approach is not always attractive for efficient coherent control schemes as the resonant Rabi oscillation period is proportional to the scalar product of the electric dipole moment times the electric field of the laser pulse. As a consequence, different excitation levels are achieved due to the intensity distribution within the focal area of a typical Gaussian laser beam and in case of molecules due to different orientations in a typical isotropic sample. This is why adiabatic strong-field approaches are especially important as they are robust against these effects.

Efficient and robust population transfer in molecular systems would have many exciting experimental applications ranging from life science to fundamental research. In life science the simultaneous excitation of all fluorophores within a focused laser pulse could trigger efficient localized photoreactions within a cell, lead to brighter images in laser-based fluorescence microscopy or even to enhanced resolution. In fundamental research all kinds of excited electronic state spectroscopy would benefit.

This is why strong-field excitation of molecules especially in solution has already attracted interest. A prominent experiment was an experiment by Shank and coworkers[77] studying fluorescence from laser dyes after chirped excitation in the weak- and strong-field regime. Whereas in the weak-field no changes in the fluorescence yield were observed, in the strong-field a fluorescence suppression was observed for negative chirp. As an explanation a frequency ordered pump–dump mechanism was offered based on theoretical considerations of Sandy Ruhman and Ronnie Kosloff.[111] Another example is the feedback optimization of fluorescence in a laser dye, where an enhancement of fluorescence was also found for positive chirped pulses by Kent Wilson and coworkers.[36] In the light of these experiments a theoretical publication by Wilson and coworkers[75] was published. In that work it was found that nearly complete electronic population inversion of molecules can be achieved with intense positively chirped broadband laser pulses, as a combined result of vibrational coherence and adiabatic inversion. Strong-field quantum calculations demonstrated inversion probabilities of up to 99%. In addition the results were shown to be robust with respect to changes in light field parameters as well as to thermal and condensed phase conditions. Similar conclusions were drawn by Ronnie Kosloff and coworkers taking a different approach: they found that a field of sufficiently high chirp rate imposes a certain relative phase between a ground and excited state wave function of a two-level system that explains the unidirectionality of the population transfer from the ground to the excited state in atomic and molecular systems.

These findings motivated our experiments on efficient and robust population transfer in sensitizer dyes.[113] Important natural pulse parameters to study strong-field effects in order to induce adiabatic population transfer are frequency sweeps and time varying intensity profiles. This is why we parameterized our excitation pulses in terms of the instantaneous frequency and temporal envelope asymmetries, *i.e.* in technical terms group delay dispersion (GDD) and third order dispersion (TOD) (see Fig. 7). We investigated two photosensitizer dyes in solution under the same experimental conditions being prepared in the triplet ground state. Excitation within the triplet system was followed by intersystem crossing and the corresponding singlet fluorescence was monitored as a measure of population transfer in the triplet system. We recorded control landscapes with respect to the fluorescence intensity on both dyes by a systematic variation of laser pulse shapes combining GDD and TOD. In the strong-field regime we found highly structured topologies with large areas of maximum or minimum population transfer that were insensitive over a certain range of applied laser intensities thus demonstrating robustness. One example is displayed in Fig. 7.

We then compared our experimental results to vibrational wave packet simulations for a molecular two-state system, where for generality two parameterized

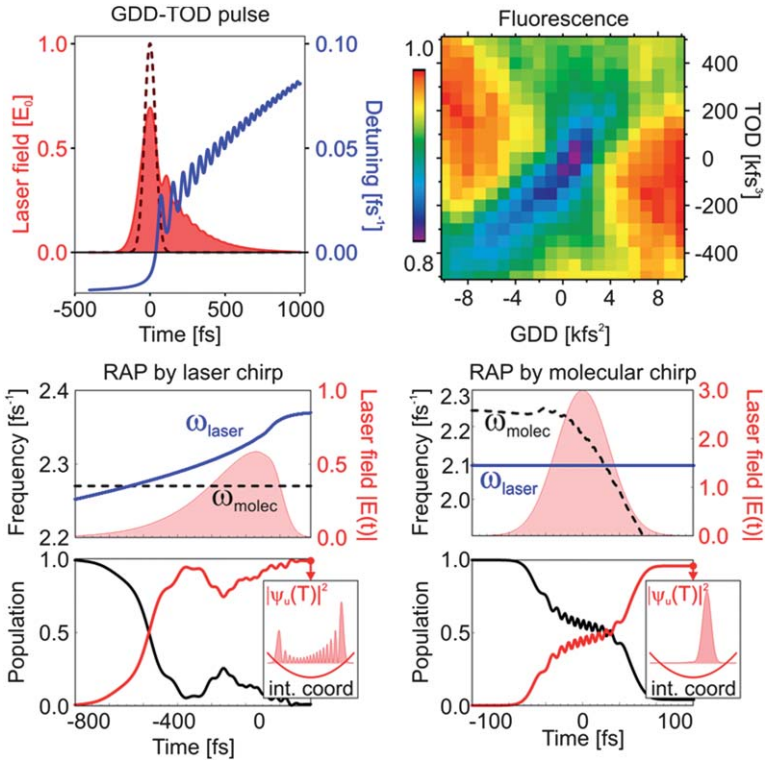

Fig. 7 Strong-field control of population transfer in a sensitizer dye in solution. Upper left: Example of a shaped femtosecond laser pulse obtained by spectral phase modulation using the phase function $\varphi(\omega) = \phi_2/2\ (\omega-\omega_0)^2 + \phi_3/6\ (\omega-\omega_0)^3$ with a GDD of $\phi_2 = 4$ kfs^2 and a TOD of $\phi_3 = 200$ kfs^3. The initial unshaped laser pulse (dashed) has a FWHM of 60 fs. Due to the combined action of GDD and TOD both the shape of the pulse envelope (red shaded) and the instantaneous laser frequency (blue) are controlled (see ref. 113 for a comprehensive discussion of GDD-TOD pulse shapes). Upper right: Measured fluorescence signal from strong-field excitation (peak intensity of the bandwidth limited pulse of about 60 GW cm^{-2}) of porphyrazine molecules as a function of GDD and TOD. A highly structured topology is observed with large areas of maximum and minimum population transfer. Lower panels: Two examples of control of population transfer in molecule. In the "RAP by laser chirp" scenario the laser frequency ω_{laser} (blue) sweeps over the molecular transition ω_{molec} (black) such that at the crossing of both curves population is adiabatically transferred from the ground sate (black) into the excited state (red). Note that after the interaction at time $T \approx 400$ fs population is transferred to the upper state with almost unit efficiency and the system is in a vibrational eigenstate of the upper potential. Alternatively, in the "RAP by molecular chirp" a bandwidth limited pulse with a constant instantaneous frequency ω_{laser} (blue) drives the molecular dynamics such that the molecular transition frequency ω_{molec} (black) sweeps over the laser frequency due to the wave packet motion inducing almost complete population transfer. In this scenario the wave packet dynamics is characterized by Joint Motion (JOMO) of the ground- and the excited-state wave packet (see ref. 113 for a detailed discussion of JOMO). Accordingly, after the interaction at time $T \approx 150$ fs, a vibrational wave packet is formed in the upper potential.

one-dimensional harmonic potentials were considered. Calculated control landscapes based on the same pulse parameters were in good accordance with experimental data for both sensitizer dyes, while different detunings of the laser central frequency to the dye absorption bands are accounted for by appropriate laser detunings in simulations. We identified areas with complete population transfer and nearly complete population return inside the landscapes, both being robust over

a wide range of intensity variations. By modelling decoherence in a simple approach, good agreement of the measured and simulated landscapes implied that coherent control of population transfer in sensitizer dyes can take place in the liquid phase, *i.e.* in the presence of decoherence in accordance with the findings by Kent Wilson and coworkers.[75]

The good agreement motivated us to analyze the physical mechanisms controlling the final state populations further in simulations. We found that atom-like interpretations of adiabatic interactions are possible. Two scenarios are presented in Fig. 7.

In one scenario the wave packet dynamics are characterized by a coupling of the ground state and excited state wave packets, inducing a joint wave packet motion (JOMO), leading to a well-defined joint internuclear distance $R(t)$. The time-dependent molecular transition frequency induced by JOMO allows for efficient population transfer when a crossing with the instantaneous frequency of the laser occurs ("RAP by molecular chirp"). Such a crossing can even be achieved when a bandwidth-limited pulse with constant instantaneous laser frequency is used. The displayed off-resonant excitation was not in the parameter space of our experiment. However, coherent population return based on JOMO was within the parameters of the experiment.[113]

The second scenario is based on the excitation of a single vibrational eigenstate by narrowband interaction in the Franck–Condon region during the weak starting part of the laser pulse. A "RAP by laser chirp" process is now observed when the instantaneous frequency of the laser is tuned over the molecular resonance during the more intense parts of the pulse.

These findings suggest, that GDD-TOD pulses are a suitable parameterization to study strong-field effects. In the light of possible applications we note, that typical peak intensities of the bandwidth limited pulses in our experiment are approximated to $I = 60$ GW cm^{-2} (taking into account that dye molecules typically provide oscillator strengths in the range of unity, the pulse area reaches 4 times 2π indicating strong-field excitation conditions). Note also that the peak field strength is reduced for shaped pulses (for analytical expressions see ref. 113) and that an applied intensity of 200 GW cm^{-2} is a value that is commonly used as the damage threshold for biological samples (see ref. 114 and references therein).

5. Control of ionization processes in dielectrics

In this last section we briefly highlight the extension of experimental control methodologies to ultrafast laser control of incoherent processes with an emphasis on processing of dielectrics on the nanometre scale. Here, primary processes induced by ultrafast laser radiation involve nonlinear electronic excitation where electron electron collisions at high excitation densities (in the range 10^{21} e cm^{-3} for ablation of dielectrics) destroy any coherence imprinted by the light field. In general, the electronic excitation is followed by energy transfer to the lattice and phase transitions that occur on fast (femtosecond, picosecond) but material-dependent time scales.[115] Optimal energy coupling with the help of suitably shaped temporal pulse envelopes thus gives the possibility to guide the material response towards user-designed directions, offering extended flexibility for quality material processing.[22] We perform prototype studies in the above mentioned spirit on dielectrics, water and metals. In dielectrics we have observed different thresholds for material processing with temporally asymmetric pulse shapes that we attributed to control of different ionization processes *i.e.* multi-photon ionization and avalanche ionization (see Fig. 8).[116–118] The resulting nanometre scale structures were one order of magnitude below the diffraction limit. Recently we extended our studies to investigate the dynamics of free electron plasma created by femtosecond pulses in a thin water jet[119] to a direct observation of the free electron density after excitation with temporally shaped laser pulses by using spectral interference techniques.[120,121] Exploiting polarization-dependent near field effects[122] is an alternative route to nanoscale

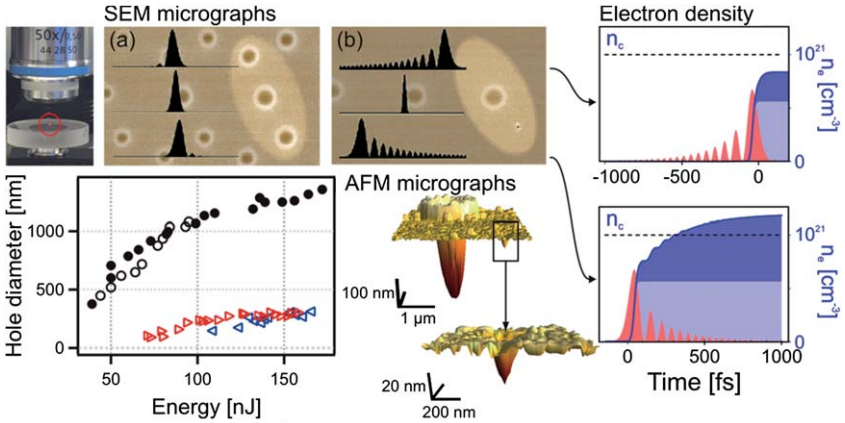

Fig. 8 Control of ionization processes in fused silica *via* asymmetrically shaped femtosecond pulses. Upper left: In our materials processing platform, a femtosecond laser pulse is focused using a microscope objective. Due to the nonlinear interaction the laser induced plasma is highly localized. Scanning electron microscope (SEM) micrographs of a measurement pattern: for an applied energy and focal position, a triplet of laser pulses is highlighted by the ellipse. Negative, zero, and positive TOD were used. Normalized temporal intensity profiles are sketched for comparison between different TODs. (a) Low TOD ($\phi_3 = \pm 2.5 \times 10^4$ fs^3, $E =$ 77 nJ) results in negligible differences between created structures. (b) High positive TOD ($\phi_3 = +6 \times 10^5$ fs^3, $E = 71$ nJ) results in a change of structure size and threshold energy (adapted from ref. 117). Diameters of ablation structures for fused silica with ($\phi_3 = 0$ fs^3, ○ and ● for two completely independent measurements confirm the reproducibility of our setup), for ($\phi_3 = +6 \times 10^5$ fs^3 (red) and ($\phi_3 = -6 \times 10^5$ fs^3 (blue)). Exemplified topology of the large structure (top) due to the unshaped pulse and the small structure (bottom) obtained by the shaped pulse measured *via* AFM. Note that this small structure is an order of magnitude below the diffraction limit. Right: Transient free electron density n_e (solid blue lines) as modeled by a simple rate equation describing multi photon ionization with k photons (σ_k) and avalanche ionization (α) *via* $dn_e/dt = \sigma_k I^k + \alpha n_e I$, together with the contributions provided by photo ionization alone $\sigma_k I^k$ (light blue shaded area) and avalanche photo ionization alone $\alpha n_e I$ (dark blue shaded area) and the corresponding electrical field (red shaded area) of the modulated pulses proportional to $I^{1/2}$. Note that the free electron density exceeds the critical value for material ablation n_c only for a positive value of ϕ_3. This observation has been discussed in a *seed and heat* mechanism based on a refined ionization model employing a multiple rate equation approach.[116]

material processing of dielectrics[123,124] Minimizing the spatial structure and at the same time maximizing the spectrochemical sensitivity for fs-LIBS[125,126] (LIBS = laser induced breakdown spectroscopy) completes our experiments exploiting temporal pulse tailoring for material processing.

6. Conclusions

In this Introductory lecture we first summarized recent developments in coherent control before we focused on our experiments on (coherent) electronic excitation with shaped femtosecond laser pulses with respect to recent developments.

We started by discussing how to make use of the electronic structure of matter together with polarization shaped laser pulses in order to create designed electron wave packets in the continuum and showed how to reconstruct the created three-dimensional electron distributions *via* tomography. We pointed out that the techniques developed open new routes to molecular recognition with an emphasis on chiral recognition in the gas phase as well as to the measurement of photoelectron angular distributions in the molecular frame.

We then turned to control of coherent electronic excitation in the Rabi cycling regime with shaped laser pulses. We highlighted the importance of controlling resonant processes under such strong-field conditions and gave two examples. In gas

phase experiments we hinted at a general strong-field scheme based on selective population of dressed states (SPODS) and especially to the consequences of controlling electronic coherences (being in the order of one femtosecond for typical valence excitations) with attosecond precision. By this, population to different final states in atoms and molecules can be switched with high selectivity and efficiency. In the liquid phase we discussed strong-field scenarios for adiabatic population transfer. In our experiments on porphyrazines we used physically motivated pulse parameterizations for adiabatic strong-field interactions. These were based on frequency sweeps together with temporal pulse envelope asymmetries. Comparison to simulations helped us to identify possible mechanisms for adiabatic population transfer in molecules. Joint wave packet motion (JOMO) and eigenstate preparation are presented as adiabatic strong-field processes complementing the well known frequency ordering followed by pump–dump scenarios and picosecond ultrabroadband positive chirp approaches.

Finally we briefly presented our experiments demonstrating control of incoherent ionization processes in dielectrics for material processing on the nanometre scale. We showed that shaping temporal asymmetric profiles address multi photon ionization and electron-electron impact ionization in a different fashion leading to different observed ablation thresholds for pulses with the same fluence, same statistical pulse duration and same focusing conditions. By this we point to a further extension of ultrafast coherent control methodologies in material processing: here optimal energy coupling with the help of suitably shaped temporal pulse envelopes gives the possibility to guide the material response towards user-designed directions, offering extended flexibility for quality material processing.

7. Acknowledgements

T.B. would like to thank Ben Whitaker, Mike Bearpark, Regina de Vivie-Riedle, Helen Fielding and Thomas Weinacht from the Scientific Committee for the invitation to give this introductory lecture and for putting such a stimulating program together. T.B. is also grateful for the lovely conference dinner including the traditional Faraday Loving Cup ceremony. Besides the authors mentioned on our publications the work presented here is mainly based on the PhD work of Tim Bayer, Lars Englert, Jens Köhler and Marc Krug with substantial experimental support by Cristian Sarpe. Financial support by DFG and the EU-ITN-FASTQUAST is acknowledged as well.

References

1 A. H. Zewail, *J. Phys. Chem.*, 2000, **104**, 5660–5694.
2 J. Manz and L. Woeste, *Femtosecond Chemistry*, VCH, Weinheim, 1995.
3 S. A. Rice and M. Zhao, *Optical control of molecular dynamics*, Wiley, New York, 2000.
4 M. Shapiro and P. Brumer, *Principles of the Quantum Control of Molecular Processes*, John Wiley & Sons, Hoboken, New Jersey, 2003.
5 D. Tannor, *Introduction to Quantum Mechanics: A Time-Dependent Perspective*, Palgrave Macmillan Publishers Limited, Houndmills, Basingstoke, Hampshire, England, 2007.
6 D. J. Tannor and S. A. Rice, *Adv. Chem. Phys.*, 1988, **70**, 441–523.
7 M. Shapiro and P. Brumer, *Int. Rev. Phys. Chem.*, 1994, **13**, 187–229.
8 T. Baumert, J. Helbing, and G. Gerber, in *Advances in Chemical Physics - Photochemistry: Chemical Reactions and their control on the Femtosecond Time Scale*, ed. I. Prigogine and S. A. Rice, John Wiley & Sons, Inc., New York, 1997, pp. 47–77.
9 H. Rabitz, R. de Vivie-Riedle, M. Motzkus and K. Kompa, *Science*, 2000, **288**, 824–828.
10 M. Shapiro and P. Brumer, *Rep. Prog. Phys.*, 2003, **66**, 859–942.
11 D. Goswami, *Phys. Rep.*, 2003, **374**, 385–481.
12 M. Dantus and V. V. Lozovoy, *Chem. Rev.*, 2004, **104**, 1813–1859.
13 V. Bonacic-Koutecky and R. Mitric, *Chem. Rev.*, 2005, **105**, 11–65.
14 T. Brixner, T. Pfeifer, G. Gerber, M. Wollenhaupt, and T. Baumert, in *Femtosecond Laser Spectroscopy*, (P. Hannaford, Ed), pp. 225–266. Springer Verlag, (2005).

15 M. Wollenhaupt, V. Engel and T. Baumert, *Annu. Rev. Phys. Chem.*, 2005, **56**, 25–56.
16 P. Nuernberger, G. Vogt, T. Brixner and G. Gerber, *Phys. Chem. Chem. Phys.*, 2007, **9**, 2470–2497.
17 J. Werschnik and E. K. U. Gross, *J. Phys. B: At., Mol. Opt. Phys.*, 2007, **40**, R175–R211.
18 W. Wohlleben, T. Buckup, J. L. Herek and M. Motzkus, *ChemPhysChem*, 2005, **6**, 850–857.
19 Y. Silberberg, *Annu. Rev. Phys. Chem.*, 2009, **60**, 277–292.
20 K. Ohmori, *Annu. Rev. Phys. Chem.*, 2009, **60**, 487–511.
21 C. Brif, R. Chakrabarti and H. Rabitz, *New J. Phys.*, 2010, **12**, 075008.
22 R. Stoian, M. Wollenhaupt, T. Baumert, and I. V. Hertel, in *Laser Precision Microfabrication*, ed. K. Sugioka, M. Meunier, and A. Piqué, Springer-Verlag, Berlin Heidelberg, 2010, pp. 121–144.
23 *Advances in Chemical Physics: Chemical Reactions and Their Control on the Femtosecond Time Scale, XXth Solvay Conference on Chemistry*, ed. P. Gaspard and I. Burghardt, John Wiley & Sons Inc., New York, 1997, vol. 101.
24 J. L. Herek, *J. Photochem. Photobiol., A*, 2006, **180**, 225.
25 H. Fielding, M. Shapiro and T. Baumert, *J. Phys. B: At., Mol. Opt. Phys.*, 2008, **41**, 070201–070201-1.
26 H. Rabitz, *New J. Phys.*, 2009, **11**, 105030.
27 H. H. Fielding and M. A. Robb, *Phys. Chem. Chem. Phys.*, 2010, **12**, 15569.
28 A. M. Weiner, *Rev. Sci. Instrum.*, 2000, **71**, 1929–1960.
29 M. Wollenhaupt, A. Assion, and T. Baumert, in *Springer Handbook of Lasers and Optics*, ed. F. Träger, Springer Science + Business Media, New York, 2007, pp. 937–983.
30 D. B. Strasfeld, S.-H. Shim and M. T. Zanni, *Adv. Chem. Phys.*, 2009, **141**, 1–28.
31 A. Monmayrant, S. Weber and B. Chatel, *J. Phys. B: At., Mol. Opt. Phys.*, 2010, **43**, 103001–103001-34.
32 J. Köhler, M. Wollenhaupt, T. Bayer, C. Sarpe and T. Baumert, *Opt. Express*, 2011, **19**, 11638–11653.
33 R. S. Judson and H. Rabitz, *Phys. Rev. Lett.*, 1992, **68**, 1500–1503.
34 T. Baumert, T. Brixner, V. Seyfried, M. Strehle and G. Gerber, *Appl. Phys. B: Lasers Opt.*, 1997, **65**, 779–782.
35 D. Meshulach, D. Yelin and Y. Silberberg, *Opt. Commun.*, 1997, **138**, 345–348.
36 C. J. Bardeen, V. V. Yakolev, K. R. Wilson, S. D. Carpenter, P. M. Weber and W. S. Warren, *Chem. Phys. Lett.*, 1997, **280**, 151–158.
37 A. Assion, T. Baumert, M. Bergt, T. Brixner, B. Kiefer, V. Seyfried, M. Strehle and G. Gerber, *Science*, 1998, **282**, 919–922.
38 R. J. Levis and H. A. Rabitz, *J. Phys. Chem. A*, 2002, **106**, 6427–6444.
39 C. Daniel, J. Full, L. Gonzáles, C. Lupulescu, J. Manz, A. Merli, S. Vajda and L. Wöste, *Science*, 2003, **299**, 536–539.
40 T. Hornung, R. Meier and M. Motzkus, *Chem. Phys. Lett.*, 2000, **326**, 445–453.
41 A. Bartelt, A. Lindinger, C. Lupulescu, S. Vajda and L. Wöste, *Phys. Chem. Chem. Phys.*, 2003, **5**, 3610–3615.
42 S. Fechner, F. Dimler, T. Brixner, G. Gerber and D. J. Tannor, *Opt. Express*, 2007, **15**, 15387–15401.
43 T. Bayer, M. Wollenhaupt and T. Baumert, *J. Phys. B: At., Mol. Opt. Phys.*, 2008, **41**, 074007–074007-13.
44 S. Ruetzel, C. Stolzenberger, F. Dimler, D. J. Tannore and T. Brixner, *Phys. Chem. Chem. Phys.*, 2011, **13**, 8627–8636.
45 M. Wollenhaupt, A. Präkelt, C. Sarpe-Tudoran, D. Liese and T. Baumert, *J. Mod. Opt.*, 2005, **52**, 2187–2195.
46 H. A. Rabitz, M. M. Hsieh and C. M. Rosenthal, *Science*, 2004, **303**, 1998–2001.
47 M. Motzkus and T. Baumert, *Symposium Quantum Control Spectroscopy (at spring meeting of Deutsche Physikalische Gesellschaft)*, 2010.
48 T. Brixner, G. Krampert, T. Pfeifer, R. Selle, G. Gerber, M. Wollenhaupt, O. Graefe, C. Horn, D. Liese and T. Baumert, *Phys. Rev. Lett.*, 2004, **92**, 208301–208301-4.
49 N. V. Vitanov, T. Halfmann, B. W. Shore and K. Bergmann, *Annu. Rev. Phys. Chem.*, 2001, **52**, 763–809.
50 B. W. Shore, *acta physica slovaca*, 2008, **58**, 243–486.
51 J. S. Melinger, S. R. Gandhi, A. Hariharan, J. X. Tull and W. S. Warren, *Phys. Rev. Lett.*, 1992, **68**, 2000–2003.
52 I. R. Sola, J. Santamaria and V. S. Malinovsky, *Phys. Rev. A: At., Mol., Opt. Phys.*, 2000, **61**, 043413–043413-7.
53 V. S. Malinovsky and J. L. Krause, *Eur. Phys. J. D*, 2001, **14**, 147–155.
54 M. Krug, T. Bayer, M. Wollenhaupt, C. Sarpe-Tudoran, T. Baumert, S. S. Ivanov and N. V. Vitanov, *New J. Phys.*, 2009, **11**, 105051.

55 S. Zhdanovich, E. A. Shapiro, M. Shapiro, J. W. Hepburn and V. Milner, *Phys. Rev. Lett.*, 2008, **100**, 103004–103004-4.
56 C. Trallero-Herrero, J. L. Cohen and T. Weinacht, *Phys. Rev. Lett.*, 2006, **96**, 063603–063603-4.
57 M. Wollenhaupt, A. Assion, O. Bazhan, C. Horn, D. Liese, C. Sarpe-Tudoran, M. Winter and T. Baumert, *Phys. Rev. A: At., Mol., Opt. Phys.*, 2003, **68**, 015401–015401-4.
58 M. Wollenhaupt, D. Liese, A. Präkelt, C. Sarpe-Tudoran and T. Baumert, *Chem. Phys. Lett.*, 2006, **419**, 184–190.
59 T. Bayer, M. Wollenhaupt, C. Sarpe-Tudoran and T. Baumert, *Phys. Rev. Lett.*, 2009, **102**, 023004–1-023004-4.
60 M. Wollenhaupt, T. Bayer, N. V. Vitanov and T. Baumert, *Phys. Rev. A: At., Mol., Opt. Phys.*, 2010, **81**, 053422–053422-9.
61 M. Wollenhaupt, A. Präkelt, C. Sarpe-Tudoran, D. Liese and T. Baumert, *Appl. Phys. B: Lasers Opt.*, 2006, **82**, 183–188.
62 J. H. Posthumus, *Rep. Prog. Phys.*, 2004, **67**, 623–665.
63 T. Frohnmeyer, M. Hofmann, M. Strehle and T. Baumert, *Chem. Phys. Lett.*, 1999, **312**, 447–454.
64 B. J. Sussman, D. Townsend, M. Y. Ivanov and A. Stolow, *Science*, 2006, **314**, 278–281.
65 T. Baumert, V. Engel, C. Meier and G. Gerber, *Chem. Phys. Lett.*, 1992, **200**, 488–494.
66 H. Goto, H. Katsuki, H. Ibrahim, H. Chiba and K. Ohmori, *Nat. Phys.*, 2011, **7**, 383–385.
67 P. Nuernberger, D. Wolpert, H. Weiss and G. Gerber, *Proc. Natl. Acad. Sci. U. S. A.*, 2010, **107**, 10366–10370.
68 D. B. Strasfeld, S.-H. Shim and M. T. Zanni, *Phys. Rev. Lett.*, 2007, **99**, 038102–038102-4.
69 J. L. Herek, W. Wohlleben, R. Cogdell, D. Zeidler and M. Motzkus, *Nature*, 2002, **417**, 533–535.
70 G. Vogt, G. Krampert, P. Niklaus, P. Nuernberger and G. Gerber, *Phys. Rev. Lett.*, 2005, **94**, 068305–068305-4.
71 V. I. Prokhorenko, A. M. Nagy, S. A. Waschuk, L. S. Brown, R. R. Birge and R. J. D. Miller, *Science*, 2006, **313**, 1257–1261.
72 T. Brixner, N. H. Damrauer, P. Niklaus and G. Gerber, *Nature*, 2001, **414**, 57–60.
73 M. Roth, L. Guyon, J. Roslund, V. Boutou, F. Courvoisier, J.-P. Wolf and H. Rabitz, *Phys. Rev. Lett.*, 2009, **102**, 253001–253001-4.
74 J. Petersen, R. Mitric, V. Bonacic-Koutecky, J.-P. Wolf, J. Roslund and H. Rabitz, *Phys. Rev. Lett.*, 2010, **105**, 073003.
75 J. Cao, C. J. Bardeen and K. R. Wilson, *Phys. Rev. Lett.*, 1998, **80**, 1406–1409.
76 J. Vala and R. Kosloff, *Opt. Express*, 2001, **8**, 238–245.
77 G. Cerullo, C. J. Bardeen, Q. Wang and C. V. Shank, *Chem. Phys. Lett.*, 1996, **262**, 362–368.
78 M. Wollenhaupt, A. Assion, D. Liese, C. Sarpe-Tudoran, T. Baumert, S. Zamith, M. A. Bouchene, B. Girard, A. Flettner, U. Weichmann and G. Gerber, *Phys. Rev. Lett.*, 2002, **89**, 173001–173001-4.
79 M. Winter, M. Wollenhaupt and T. Baumert, *Opt. Commun.*, 2006, **264**, 285–292.
80 F. Lindner, M. G. Schätzel, H. Walther, A. Baltuska, E. Goulielmakis, F. Krausz, D. B. Milosevic, D. Bauer, W. Becker and G. G. Paulus, *Phys. Rev. Lett.*, 2005, **95**, 040401–040401-4.
81 S. H. Autler and C. H. Townes, *Phys. Rev.*, 1955, **100**, 703–722.
82 M. Wollenhaupt, A. Präkelt, C. Sarpe-Tudoran, D. Liese, T. Bayer and T. Baumert, *Phys. Rev. A: At., Mol., Opt. Phys.*, 2006, **73**, 063409–063409-15.
83 M. Wollenhaupt, M. Krug, J. Köhler, T. Bayer, C. Sarpe-Tudoran and T. Baumert, *Appl. Phys. B: Lasers Opt.*, 2009, **95**, 245–259.
84 A. T. J. B. Eppink and D. H. Parker, *Rev. Sci. Instrum.*, 1997, **68**, 3477–3484.
85 *Imaging in Molecular Dyanmics - Technology and Applications*, ed. B. Whitaker, Cambridge University Press, Cambridge, 2003.
86 C. Bordas, F. Pauling, H. Helm and D. L. Huestis, *Rev. Sci. Instrum.*, 1996, **67**, 2257–2268.
87 M. J. J. Vrakking, *Rev. Sci. Instrum.*, 2001, **72**, 4084–4089.
88 V. Dribinski, A. Ossadtchi, V. A. Mandelshtam and H. Reisler, *Rev. Sci. Instrum.*, 2002, **73**, 2634–2642.
89 G. A. Garcia, L. Nahon and I. Powis, *Rev. Sci. Instrum.*, 2004, **75**, 4989–4996.
90 M. Wollenhaupt, M. Krug, J. Köhler, T. Bayer, C. Sarpe-Tudoran and T. Baumert, *Appl. Phys. B: Lasers Opt.*, 2009, **95**, 647–651.
91 M. Krug, PhD thesis, Kohärente Kontrolle winkelaufgelöster Photoelektronenspektren, Universität Kassel, 2010.
92 A. Stolow, A. E. Bragg and D. M. Neumark, *Chem. Rev.*, 2004, **104**, 1719–1757.
93 C. Smeenk, L. Arissian, A. Staude, D. M. Villeneuve and P. B. Corkum, *J. Phys. B: At., Mol. Opt. Phys.*, 2009, **42**, 165402.

94 H. Stapelfeldt and T. Seideman, *Rev. Mod. Phys.*, 2003, **75**, 543–557.
95 C. Horn, M. Wollenhaupt, M. Krug, T. Baumert, R. de Nalda and L. Banares, *Phys. Rev. A: At., Mol., Opt. Phys.*, 2006, **73**, 031401–031401-4.
96 J. Ullrich, R. Moshammer, A. Dorn, R. Dörner, L. Ph, H. Schmidt and H. Schmidt-Böcking, *Rep. Prog. Phys.*, 2003, **66**, 1463–1545.
97 A. Vredenborg, W. G. Roeterdink and M. H. M. Janssen, *Rev. Sci. Instrum.*, 2008, **79**, 063108.
98 *Chiral Recognition in the Gas Phase*, ed. A. Zehnacker, CRC Press, Boca Raton FL USA, 2010.
99 L. Nahon, G. A. Garcia, C. J. Harding, E. Mikajlo and I. Powis, *J. Chem. Phys.*, 2006, **125**, 114309.
100 X. Li and M. Shapiro, *J. Chem. Phys.*, 2010, **132**, 194315.
101 M. Wollenhaupt, A. Präkelt, C. Sarpe-Tudoran, D. Liese and T. Baumert, *J. Opt. B: Quantum Semiclassical Opt.*, 2005, **7**, S270–S276.
102 R. Hildner, D. Brinks and N. F. van Hulst, *Nature Physics*, 2010, 1–6.
103 N. Dudovich, T. Polack, A. Péer and Y. Silberberg, *Phys. Rev. Lett.*, 2005, **94**, 083002–083002-4.
104 M. Wollenhaupt and T. Baumert, *J. Photochem. Photobiol., A*, 2006, **180**, 248–255.
105 S. R. Hartmann and E. L. Hahn, *Phys. Rev.*, 1962, **128**, 2053.
106 E. T. Sleva, I. M. Xavier Jr. and A. H. Zewail, *J. Opt. Soc. Am. B*, 1985, **3**, 483–487.
107 Y. S. Bai, A. G. Yodh and T. W. Mossberg, *Phys. Rev. Lett.*, 1985, **55**, 1277–1280.
108 E. Goulielmakis, Z.-H. Loh, A. Wirth, R. Santra, N. Rohringer, V. S. Yakovlev, S. Zherebtsov, T. Pfeifer, A. M. Azzeer, M. F. Kling, S. R. Leone and F. Krausz, *Nature*, 2010, **466**, 739–743.
109 M. Wollenhaupt, T. Bayer, A. Klumpp, C. Sarpe-Tudoran, and T. Baumert, in *Springer Proceedings in Physics 127 (Physics and Engineering of New Materials)*, ed. D. T. Cat, A. Pucci, and K. Wandelt, Springer, 2008, pp. 327–335.
110 R. Kosloff, A. D. Hammerich and D. Tannor, *Phys. Rev. Lett.*, 1992, **69**, 2172–2175.
111 S. Ruhman and R. Kosloff, *J. Opt. Soc. Am. B*, 1990, **7**, 1748–1752.
112 C.-M. Simon, T. Belhadj, B. Chatel, T. Amand, A. Lemaitre, O. Krebs, P. A. Dalgarno, R. J. Warburton, X. Marie and B. Urbaszek, *Phys. Rev. Lett.*, 2011, **106**, 166801.
113 J. Schneider, M. Wollenhaupt, A. Winzenburg, T. Bayer, J. Köhler, R. Faust and T. Baumert, *Phys. Chem. Chem. Phys.*, 2011, **13**, 8733–8746.
114 K. E. Sheetz and J. Squier, *J. Appl. Phys.*, 2009, **105**, 051101.
115 B. Rethfeld, K. Sokolowski-Tinten, D. von der Linde and S. I. Anisimov, *Appl. Phys. A: Mater. Sci. Process.*, 2004, **79**, 767–769.
116 L. Englert, B. Rethfeld, L. Haag, M. Wollenhaupt, C. Sarpe-Tudoran and T. Baumert, *Opt. Express*, 2007, **15**, 17855–17862.
117 L. Englert, M. Wollenhaupt, L. Haag, C. Sarpe-Tudoran, B. Rethfeld and T. Baumert, *Appl. Phys. A: Mater. Sci. Process.*, 2008, **92**, 749–753.
118 M. Wollenhaupt, L. Englert, A. Horn and T. Baumert, *J. Laser Micro/Nanoeng.*, 2009, **4**, 144–151.
119 C. Sarpe-Tudoran, A. Assion, M. Wollenhaupt, M. Winter and T. Baumert, *Appl. Phys. Lett.*, 2006, **88**, 261109–261109-3.
120 E. Tokunaga, A. Terasaki and T. Kobayashi, *Opt. Lett.*, 1992, **17**, 1131–1133.
121 V. V. Temnov, K. Sokolowski-Tinten, P. Zhou, A. El-Khamhawy and D. von der Linde, *Phys. Rev. Lett.*, 2006, **97**, 237403–237403-4.
122 M. Aeschlimann, M. Bauer, D. Bayer, T. Brixner, F. J. García de Abajo, W. Pfeiffer, M. Rohmer, C. Spindler and F. Steeb, *Nature*, 2007, **446**, 301–304.
123 F. Hubenthal, R. Morarescu, L. Englert, L. Haag, T. Baumert and F. Träger, *Appl. Phys. Lett.*, 2009, **95**, 063101–063101-3.
124 R. Morarescu, L. Englert, B. Kolaric, P. Damman, R. A. L. Vallée, T. Baumert, F. Hubenthal and F. Träger, *J. Mater. Chem.*, 2011, **21**, 4076–4081.
125 A. Assion, M. Wollenhaupt, L. Haag, F. Mayorov, C. Sarpe-Tudoran, M. Winter, U. Kutschera and T. Baumert, *Appl. Phys. B: Lasers Opt.*, 2003, **77**, 391–397.
126 W. Wessel, A. Brückner-Foit, J. Mildner, L. Englert, L. Haag, A. Horn, M. Wollenhaupt and T. Baumert, *Eng. Fract. Mech.*, 2010, **77**, 1874–1883.

